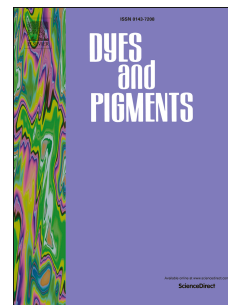


Accepted Manuscript

Derivatives of 2-phenylindole and carbazole as host materials for phosphorescent organic light emitting diodes

Rasa Keruckiene, Dmytro Volyniuk, Jolita Ostrauskaite, Laura Peculyte, Juozas V. Grazulevicius, Sergei V. Kostjuk, Algirdas Lazauskas



PII: S0143-7208(16)30738-0

DOI: [10.1016/j.dyepig.2016.09.038](https://doi.org/10.1016/j.dyepig.2016.09.038)

Reference: DYPI 5490

To appear in: *Dyes and Pigments*

Received Date: 27 June 2016

Revised Date: 13 September 2016

Accepted Date: 15 September 2016

Please cite this article as: Keruckiene R, Volyniuk D, Ostrauskaite J, Peculyte L, Grazulevicius JV, Kostjuk SV, Lazauskas A, Derivatives of 2-phenylindole and carbazole as host materials for phosphorescent organic light emitting diodes, *Dyes and Pigments* (2016), doi: 10.1016/j.dyepig.2016.09.038.

This is a PDF file of an unedited manuscript that has been accepted for publication. As a service to our customers we are providing this early version of the manuscript. The manuscript will undergo copyediting, typesetting, and review of the resulting proof before it is published in its final form. Please note that during the production process errors may be discovered which could affect the content, and all legal disclaimers that apply to the journal pertain.

DERIVATIVES OF 2-PHENYLINDOLE AND CARBAZOLE AS HOST MATERIALS FOR PHOSPHORESCENT ORGANIC LIGHT EMITTING DIODES

Rasa Keruckiene¹, Dmytro Volyniuk¹, Jolita Ostrauskaite¹, Laura Peciulyte¹, Juozas V. Grazulevicius^{1*}, Sergei V. Kostjuk², Algirdas Lazauskas³

¹*Department of Polymer Chemistry and Technology, Kaunas University of Technology, Radvilenu pl.19, LT-50254 Kaunas, Lithuania*

²*Research Institute for Physical Chemical Problems of the Belarusian State University, 14 Leningradskaya st., 220030 Minsk, Belarus.*

³*Institute of Materials Science, Kaunas University of Technology, Barsausko 59, LT-51423, Kaunas, Lithuania*

Abstract

Synthesis and thermal, electrochemical, photophysical and charge-transporting properties of the derivatives of carbazole and 2-phenylindole are reported. Compounds with reactive functional groups are emphasized. Two compounds form molecular glasses with the glass transition temperatures of 57 °C and 134 °C. The synthesized compounds absorb electromagnetic radiation in the range of 200–375 nm and emit in the range of 350–550 nm. Their solutions exhibit Stokes shifts up to 81 nm. Their triplet energy levels were found to be in the range of 2.88–3.04 eV. The ionization potentials of the synthesized compounds were found to range from 5.45 eV to 5.88 eV. The ability of photopolymerization in the solid state of the synthesized monomers was demonstrated by ATR-FTIR spectroscopy. The charge transporting properties were studied by the space-charge-limited current (SCLC) method. The zero-field hole mobilities reaching $1.97 \times 10^{-5} \text{ cm}^2 \text{ V}^{-1} \text{ s}^{-1}$ were observed. According to the results of characterization, two compounds were selected for studying them as the hosts in blue and green phosphorescent organic light emitting diodes. The

* Corresponding author. Tel.: +370 37 300193; fax: +370 37 300152. Email: juozas.grazulevicius@ktu.lt

best fabricated device consisting of indium tin oxide anode, hole-transporting layer, emitting layer with 3-((1-(4-vinylbenzyl)-2-phenyl-1H-indol-3-yl)methyl)-9-ethyl-9H-carbazole as a host and the green emitter, electron transporting layer and calcium layer topped with aluminum layer as cathode, exhibited the maximum current, power, and external quantum efficiencies of 10.3 cd/A, 7.2 lm/W, 2.9 %, respectively, in the absence of light out-coupling enhancement. The devices based on the twin derivatives of 2-phenylindolylcarbazolymethane demonstrated the relatively low values of the turn-on voltages of 3.7 and 3.1 V as well as the efficiency roll-offs of 12.5 and 22.7 %.

Keywords: indole, carbazole, phosphorescence, PHOLED.

Introduction

Phosphorescent organic light emitting diodes (OLEDs) are a prime focus of organic light emitting device research due to their high light-emitting efficiency efficiencies [1]. The efficiencies of light emission from fluorescent OLEDs are limited compared to that from OLEDs with phosphorescent (triplet) emitters. In a device without triplet emitters only the singlet excitons can be as high as 100% since the triplet emitters can harvest both singlet and triplet excitons [2]. The selection of high-triplet-energy host materials is of great importance for the preparation of efficient phosphorescent OLEDs [3]. Effective charge transport, good thermal stability, high triplet energy, capability of glass formation are the reasons why electron-rich carbazole moieties are widely used in the design of electroactive compounds [4,5]. Derivatives of carbazole with electronically isolated electroactive groups exhibit high triplet energies [6]. They showed good performance as host materials of blue phosphorescent OLEDs [7,8]. Derivatives of indole were also reported to exhibit high triplet energies [9]. However, their applicability in phosphorescent OLEDs is much less explored.

The strategy of this work was to combine carbazole and indole moieties in the design and synthesis of host materials for phosphorescent OLEDs exhibiting high triplet energy values, charge-transporting and glass-forming abilities. A series of new derivatives of 2-phenylindole and carbazole were synthesized and studied. The materials with the most suitable sets of the properties were tested as host materials in green phosphorescent light emitting diodes.

Experimental

Materials

2-Phenylindole-3-carbaldehyde, 2-phenylindole, potassium *tert*-butoxide, iron (III) chloride, zinc, titanium tetrachloride, sodium carbonate, tetrabutylammonium hexafluorophosphate, benzyltrimethylammonium chloride (BTMAC), 4-vinylbenzylchloride, bromoethane, epichlorohydrin, 9-ethylcarbazole, cyclopentadienyl(fluorene)iron(II)hexafluorophosphate, boron trifluoride diethyl etherate (all from Aldrich), 9*H*-carbazole (Reakhim) were used as received. 3-Hydroxymethyl-2-phenylindole (**HMPI**) was synthesized as described before [10].

3-((9*H*-Carbazol-3-yl)(2-phenyl-1*H*-indol-3-yl)methyl)-9*H*-carbazole (**CPIC**). To a mixture of 9*H*-carbazole (5 g, 30 mmol) and 2-phenylindole-3-carbaldehyde (3.3 g, 15 mmol) in chloroform (40mL), hydrochloric acid (conc., 5 ml) was added dropwise and the reaction mixture was stirred at room temperature for 8 h. Then, water (10 mL) was added to quench the reaction and the mixture was stirred vigorously for the additional 10 min. The crude product was extracted with chloroform several times. The chloroform solution was washed with water, dried with anhydrous sodium sulphate, filtered and the solvent was evaporated. The product was purified by silica gel column chromatography using hexane:ethylacetate (1:6) as an eluent. Yield of reddish powder was 4.5 g (56 %). $M_w = 537$ g/mol. $C_{39}H_{27}N_3$. 1H NMR (400 MHz, $CDCl_3$) δ 8.34 (s, 3H, NH), 8.23 – 7.72 (m, 9H, Ar.), 7.60 – 7.48 (m, 14H, Ar.), 5.41 (s, 1H, Ar-CH). ^{13}C NMR (101 MHz, $CDCl_3$) δ 139, 126, 124, 119, 50.

Bis(2-phenyl-1*H*-indol-3-yl)methane (**BPIM**). To a mechanically stirred solution of 3-hydroxymethyl-2-phenylindole (1.3 g 5.8 mmol) and 2-phenylindole (1.12 g, 5.8 mmol) in dry dichloromethane (40 ml), boron trifluoride diethyl etherate (3.2 ml) was added dropwise and the reaction mixture was stirred at room temperature for 3 h. The crude product was extracted with dichloromethane several times. The dichloromethane solution was washed with water, dried with anhydrous sodium sulphate, filtered and the solvent was evaporated. The product was purified by silica gel column chromatography using hexane:ethylacetate (1:9) as an eluent. Yield of greenish powder was 1.1 g (62 %). $M_w=398$ g/mol. $C_{29}H_{22}N_2$. 1H NMR (400 MHz, $CDCl_3$) δ 8.33 (s, 2H, NH), 8.00 – 7.74 (m, 18H, Ar.), 5.41 (s, 2H, Ar-CH). ^{13}C NMR (101 MHz, $CDCl_3$) δ 141, 137, 129, 127, 126, 123, 121, 119, 22.

3-((2-Phenyl-1*H*-indol-3-yl)methyl)-9*H*-carbazole (**PIMC**). To a mechanically stirred solution of 3-hydroxymethyl-2-phenylindole (1.3 g 5.8 mmol) and 9-ethylcarbazole (1.5 g, 5.8 mmol) in dry dichloromethane (40 ml), boron trifluoride diethyl etherate (3.2 ml) was added dropwise and the reaction mixture was stirred at room temperature for 3 h. The crude product was extracted with dichloromethane several times. The dichloromethane solution was washed with water, dried with anhydrous sodium sulphate, filtered and the solvent was evaporated. The product was purified by silica gel column chromatography using hexane:ethylacetate (1:9) as an eluent. Yield of greenish powder was 1.3 g (58 %). $M_w=400$ g/mol. $C_{29}H_{24}N_2$. 1H NMR (400 MHz, $CDCl_3$) δ 10.01 (s, 1H, NH), 8.00 – 7.74 (m, 9H), 7.43 – 7.15 (m, 7H), 5.69 (s, 2H, Ar-CH), 4.04 (q, 2H, $J = 7.1$ Hz, CH₂), 1.32 (t, 3H, $J = 7.1$ Hz, CH₃). ^{13}C NMR (101 MHz, $CDCl_3$) δ 141, 137, 133, 128, 121, 118, 112, 111, 108, 37, 30, 14.

9-(4-Vinylbenzyl)-3-((1-(4-vinylbenzyl))-2-phenyl-indol-3-yl)(9-(4-vinylbenzyl)-carbazol-3-yl)methyl)-carbazole (**1**) was prepared by the procedure similar to that described elsewhere[11]. To a mechanically stirred mixture of 3-((9*H*-carbazol-3-yl)(2-phenyl-1*H*-indol-3-yl)methyl)-9*H*-carbazole (**CPIC**) (0.7 g, 1.3 mmol), dimethyl sulphoxide (DMSO) (10 ml), potassium *tert*-

butoxide (0.04 g, 0.4 mmol), BTMAC (0.04 g, 0.01 mmol) and 4-vinylbenzylchloride (1 ml, 7.8 mmol) were added. The resulting mixture was stirred at room temperature for 2 h. The reaction was stopped by adding water and neutralized with 10% HCl (8 ml) to pH 6–7. The crude product was extracted with chloroform several times (50 ml×3). The chloroform solution was washed with water, dried with anhydrous sodium sulphate, filtered and the solvent was evaporated. The product was purified by silica gel column chromatography using hexane as an eluent. Yield of reddish powder was 0.86 g (75 %). $M_w = 886$ g/mol. $C_{66}H_{51}N_3$. 1H NMR (400 MHz, $CDCl_3$) δ 8.23 – 7.72 (m, 9H, Ar.), 7.60 – 7.48 (m, 14H, Ar.), 7.21 – 7.07 (m, 12H), 6.62 (m, 3H, AMX system $\underline{CH=CH_2}$ proton H^A), 5.67 (dd, 3H, AMX system $-\underline{CH=CH_2}$ proton H^M trans $J_{AM}=5.75$ Hz and gem $J_{MX}=5.80$ Hz), 5.41 (s, 1H, Ar- \underline{CH}), 5.18 (d, 3H, AMX system of $-\underline{CH=CH_2}$ proton H^X cis $J_{AX}=11$ Hz), 3.39 (s, 6H, $\underline{CH_2}$). ^{13}C NMR (101 MHz, $CDCl_3$) δ 139, 125, 123, 119, 110, 50, 45. FT-IR (KBr) cm^{-1} : 3050 (ν C–H Ar), 2919 (ν C–H aliph.), 1450 (ν C=C Ar), 1363 (ν C–N Ar), 995, 928 (C–H of vinyl group), 841, 820, 745 (γ C–H Ar). Elemental analysis for $C_{66}H_{51}N_3$. % Calc.: C, 89.46; H, 5.80; N, 4.74; % Found: C, 89.41; H, 5.85; N, 4.69. MS: m/z 886 [M^+].

9-((Oxiran-2-yl)methyl)-3-((1-((oxiran-2-yl)methyl)-2-phenyl-indol-3-yl)(9-((oxiran-2-yl)methyl)-carbazol-3-yl)methyl)-carbazole (**2**). A solution of 3-((9H-carbazol-3-yl)(2-phenyl-1H-indol-3-yl)methyl)-9H-carbazole (**CPIC**) (0.7 g, 1.3 mmol) potassium in epichlorohydrin (4 ml, 51 mmol) was stirred at 120 °C for 24 h under argon atmosphere. Then epichlorohydrin was removed by distillation. The product was purified by silica gel column chromatography using hexane as an eluent. It was recrystallized from methanol. Yield of reddish crystals was 0.74 g (81 %). M.p. 110 °C (DSC). $M_w = 705$ g/mol. $C_{48}H_{39}N_3O_3$. 1H NMR (400 MHz, $CDCl_3$) δ 7.88 (d, 9H, $J = 7.8$ Hz, Ar.), 7.28 – 7.22 (m, 7H, Ar.), 7.1–7.0 (m, 7H, Ar.), 5.07 (s, 1H, Ar- \underline{CH}), 4.40 (dd, 6H, $J = 15.8$, $J = 3.4$ Hz, $\underline{CH_2}$), 4.18 (dd, 4H, $J = 15.8$, $J = 8.1$ Hz, $\underline{CH_2}$), 3.12 (d, 2H, $J = 6.4$ Hz, $\underline{CH_2}$), 2.57 (t, 3H, $J = 4.1$ Hz, \underline{CH}). ^{13}C NMR (101 MHz, $CDCl_3$) δ 140, 125, 123, 119, 109, 50, 45. FT-IR (KBr) cm^{-1} : 3052 (ν C–H Ar), 2920 (ν C–H aliph.), 1453 (ν C=C Ar), 1351 (ν C–N Ar), 1220 (ν C–O–C), 841,

779 (γ C–H Ar). Elemental analysis for $C_{48}H_{39}N_3O_3$. % Calc.: C, 81.68; H, 5.57; N, 5.95; O, 6.80; % Found: C, 81.63; H, 5.52; N, 5.90; O, 6.85. MS: m/z 706 [(M+H)⁺].

9-Ethyl-3-((1-ethyl-2-phenyl-1H-indol-3-yl)(9-ethyl-9H-carbazol-3-yl)methyl)-9H-carbazole (3).

To a mechanically stirred mixture of 3-((9H-carbazol-3-yl)(2-phenyl-1H-indol-3-yl)methyl)-9H-carbazole (CPIC) (0.7 g, 1.3 mmol), dimethylsulfoxide (10 ml), potassium *tert*-butoxide (0.44 g, 3.9 mmol), BTMAC (0.04 g, 0.01 mmol) and bromoethane (0.58 ml, 7.8 mmol) were added. The resulting mixture was stirred at room temperature for 2 h. The reaction was stopped by adding water and neutralized with 10% HCl (8 ml) to pH 6–7. The crude product was extracted with chloroform several times (50 ml \times 3). The chloroform solution was washed with water, dried with anhydrous sodium sulphate, filtered and the solvent was evaporated. The product was purified by silica gel column chromatography using hexane as an eluent. Yield of reddish powder was 0.53 g (66 %). $M_w = 621$ g/mol. $C_{45}H_{39}N_3$. ¹H NMR (400 MHz, CDCl₃) δ 7.89 (d, 9H, $J = 7.8$ Hz, Ar.), 7.38 – 7.29 (m, 7H, Ar.), 7.2 – 7.11 (m, 7H, Ar.), 5.20 (s, 1H, Ar-CH), 4.02 (q, 6H, $J = 7.3$ Hz, CH₂), 1.32 (t, 9H, $J = 7.1$ Hz, CH₃). ¹³C NMR (101 MHz, CDCl₃) δ 139, 125, 123, 119, 110, 50, 45. FT-IR (KBr) cm^{-1} : 3052 (ν C–H Ar), 2925 (ν C–H aliph.), 1492, 1450 (ν C=C Ar), 1358 (ν C–N Ar), 842, 745 (ν C–H Ar). Elemental analysis for $C_{45}H_{39}N_3$. % Calc.: C, 86.92; H, 6.32; N, 6.76; % Found: C, 86.87; H, 6.37; N, 6.71. MS: m/z 635 [(M+Na)⁺].

1-(4-Vinylbenzyl)-3-((1-(4-vinylbenzyl)-3,7-dihydro-2-phenyl-1H-indol-3-yl)methyl)-2-phenyl-1H-indole (4). To a mechanically stirred solution of bis(2-phenyl-1H-indol-3-yl)methane (BPIM) (1.5 g, 3.7 mmol) in dimethylsulfoxide (10 ml), potassium *tert*-butoxide (1.26 g, 11.3 mmol), BTMAC (0.04g, 0.01 mmol) and 4-vinylbenzylchloride (2.1 ml, 15.6 mmol) were added. The resulting mixture was stirred at room temperature for 2 h. The reaction was stopped by adding water and neutralized with 10% HCl (8 ml) to pH 6–7. The crude product was extracted with chloroform several times (50 ml \times 3). The chloroform solution was washed with water, dried with anhydrous sodium sulphate, filtered and the solvent was evaporated. The product was purified by silica gel

column chromatography using hexane as an eluent. Yield of greenish crystals was 1.7 g (74 %). M.p. 120°C (DSC). $M_w=632$ g/mol. $C_{47}H_{40}N_2$. 1H NMR (400 MHz, $CDCl_3$) δ 8.05 (d, 8H, $J = 7.8$, Ar.), 8.00 – 7.74 (m, 18H, Ar.), 6.62 (m, 2H, AMX system $\underline{CH=CH_2}$ proton H^A), 5.61 (dd, 2H AMX system $-CH=\underline{CH_2}$ proton H^M trans $J_{AM}=16.2$ Hz and gem $J_{MX}=8.40$), 5.41 (s, 2H, Ar- \underline{CH}), 5.26 (d, 2H, AMX system of $-CH=\underline{CH_2}$ proton H^X cis $J_{AX}=12.7$ Hz), 5.14 – 5.07 (m, 2H, AMX system of $-CH=\underline{CH_2}$ proton H^X), 3.38 (s, 4H, $\underline{CH_2}$). ^{13}C NMR (101 MHz, $CDCl_3$) δ 140, 137, 128, 127, 125, 123, 121, 116, 46, 41, 23. FT-IR (KBr) cm^{-1} : 3052 (ν C–H Ar), 2927 (ν C–H aliph.), 1485, 1450 (ν C=C Ar), 1381 (ν C–N Ar), 994, 969, 927 (C–H of vinyl group), 842, 785, 746 (γ C–H Ar). Elemental analysis for $C_{47}H_{40}N_2$. % Calc.: C, 89.20; H, 6.37; N, 4.43; % Found: C, 89.15; H, 6.41; N, 4.48. MS: m/z 633 [(M+H) $^+$].

3-((1-(4-Vinylbenzyl)-2-phenyl-1H-indol-3-yl)methyl)-9-ethyl-9H-carbazole (5). To a mechanically stirred solution of 3-((2-phenyl-1H-indol-3-yl)methyl)-9H-carbazole (PIMC) (2 g, 5 mmol) in dimethylsulfoxide (10 ml), potassium *tert*-butoxide (1.68 g, 15 mmol), BTMAC (0.04g, 0.01 mmol) and 4-vinylbenzylchloride (1.4 ml, 10 mmol) were added. The resulting mixture was stirred at room temperature for 2 h. The reaction was stopped by adding water and neutralized with 10% HCl (8 ml) to pH 6–7. The crude product was extracted with chloroform several times (50 ml \times 3). The chloroform solution was washed with water, dried with anhydrous sodium sulphate, filtered and the solvent was evaporated. The product was purified by silica gel column chromatography using hexane as an eluent. Yield of greenish powder was 1.7 g (68 %). $M_w=516$ g/mol. $C_{38}H_{32}N_2$. 1H NMR (400 MHz, $CDCl_3$) δ 8.13 – 8.01 (m, 2H), 8.00 – 7.74 (m, 9H), 7.43 – 7.15 (m, 7H), 6.69 – 6.51 (m, 1H, AMX system $\underline{CH=CH_2}$ proton H^A), 5.69 (s, 2H, Ar- \underline{CH}), 5.66 – 5.54 (m, 1H, AMX system of $-CH=\underline{CH_2}$ proton H^X cis), 5.22 – 5.05 (m, 1H, AMX system of $-CH=\underline{CH_2}$ proton H^X), 4.04 (q, 2H, $J = 7.1$ Hz, $\underline{CH_2}$), 3.40 (s, 2H), 1.32 (t, 3H, $J = 7.1$ Hz, $\underline{CH_3}$). ^{13}C NMR (101 MHz, $CDCl_3$) δ 141, 137, 130, 129, 125, 121, 120, 116, 111, 38, 22. FT-IR (KBr) cm^{-1} : 3052 (ν C–H Ar), 2925 (ν C–H aliph.), 1480, 1452 (ν C=C Ar), 1359 (ν C–N Ar), 993, 969, 926 (C–

H of vinyl group), 842, 745 (γ C–H Ar). Elemental analysis for $C_{38}H_{32}N_2$. % Calc.: C, 88.34; H, 6.24; N, 5.42; % Found: C, 88.394; H, 6.29; N, 5.38. MS: m/z 540 [(M+Na)⁺].

Photopolymerization of monomers **1** and **4** was performed using an UV lamp OmniCure® S2000 (Lumen Dynamics). The solution of a monomer containing 3 mol % of photoinitiator cyclopentadienyl(fluorene)iron(II)hexafluorophosphate was drop-casted on the surface of ATR crystal and the decrease of the intensity of a signal of reactive functional group under exposure of UV radiation source was monitored.

Polymerization monomer **5** was carried out in the solution of dry dichloromethane (0.5 mol/l) under argon blanket. After dissolving the monomer, initiator $BF_3 \cdot (C_2H_5)_2O$ (0.15 mol/l) was added dropwise. The reaction was carried out for 3 days and monitored by TLC (eluent: dichloromethane). The initiator was neutralized with NH_3 (aq) and the reaction product was precipitated in methanol. The precipitate was washed with methanol several times and dried.

Instrumentation

1H and ^{13}C NMR spectra were obtained using a Bruker Avance III (400 MHz). The data are given as chemical shifts (δ) in ppm against trimethylsilane (in parenthesis: multiplicity, integration, coupling constant). IR spectra were recorded using a Vertex 70 Bruker spectrometer. Mass spectra were obtained on a Waters ZQ 2000 mass spectrometer (electrospray ionization). Elemental analyses were performed with an Exeter Analytical CE-440 Elemental Analyzer. UV-vis spectra of the dilute THF solutions (10^{-4} mol/l) of the synthesized compounds were recorded with a Perkin Elmer Lambda 35 spectrophotometer. Fluorescence spectra of the dilute tetrahydrofuran solutions (10^{-4} mol/l) of the synthesized materials were recorded at room temperature and phosphorescence spectra of the the dilute tetrahydrofuran solutions (10^{-4} mol/l) were recorded at 77 K with luminescent spectrometer Edinburgh Instruments FLS980 spectrometer (excitation wavelength λ_{ex} = 320 nm). Differential scanning calorimetry (DSC) measurements were carried out using a TA Instruments Q2000 thermosystem. The samples were examined at a heating/cooling rate of 10

°C/min under nitrogen atmosphere. Thermogravimetric analysis (TGA) was performed on a TA Instruments Q50. The heating rate was 20 °C/min under nitrogen atmosphere. The melting points of the compounds were determined using an Electrothermal MEL-TEMP. Molecular weights of the polymers were determined by gel chromatography using Waters SEC system with Waters 501 UV detector and polystyrene standards.

The ionization potentials (I_p) were estimated by the electron photoemission in air method as reported earlier [12,13]. The samples for the measurements were prepared by casting chloroform solutions of the compounds onto pre-cleaned indium tin oxide (ITO) coated glass substrates.

Cyclic voltammetry measurements were performed using a glassy carbon working electrode (disk with the diameter of 2 mm) in a three-electrode cell using an Autolab Type potentiostat - galvanostat. The measurements were carried out for the solutions in dry dichloromethane containing 0.1 M tetrabutylammonium hexafluorophosphate at 25 °C, scan rate 50 mV/s, sample concentration 10^{-3} M. The potentials were measured against Ag/AgNO₃ as reference electrode. Platinum wire was used as a counter electrode. The potentials were calibrated with the standard ferrocene/ferrocenium (Fc/Fc⁺) redox system [14].

DFT calculations employing the B3LYP functional were performed with the Spartan'14 program [15]. Neutral, cationic and triplet state geometries of molecules in vacuum were optimized from conformational analysis data using 6-31G (d,p) basis set as a starting point. The HOMO/LUMO orbitals were calculated at the B3LYP/6-31G (d, p) level.

Phosphorescent OLEDs (PhOLEDs) were fabricated by thermal vacuum deposition under the vacuum higher than $3 \cdot 10^{-6}$ mBar. The host:guest emission layers were deposited by co-deposition of host (m/m 90%) (compound **2** or **5**) and dopant (m/m 10%) (tris[2-phenylpyridinato-C₂,N]iridium(III) (Ir(ppy)₃)) from two different sources. The deposition rate of guest was of 0.1 Å/s, while the deposition rate of hosts was set 1.0 Å/s. A Keithley source meter 2400-C was utilized for recording of the current density–voltage characteristics of the devices. The current density–

luminance characteristics were estimated using a calibrated silicon photodiode with the 6517B Keithley electrometer. Electroluminescence (EL) spectra were recorded by an Avantes AvaSpec-2048XL spectrometer. The current, power and external quantum efficiencies were estimated utilizing the current density, luminance, and EL spectra as reported earlier. [16]

Hole-only devices were fabricated for the space-charge-limited current (SCLC) experiments. The indium tin oxide (ITO) coated glass substrates with a sheet resistance of 15 Ω /sq were cleaned in acetone and isopropyl alcohol ultrasonic baths for ca. 5 min before depositing functional layers. Organic and metal layers were vacuum-deposited using the same conditions as for preparation of PhOLEDs. The thickness of thin films was monitored during the deposition using a quartz crystal microbalance. The sample area was 6 mm² with 7 devices per substrate.

The surface morphology of light-emitting layers was investigated by atomic force microscopy (AFM). AFM experiments were carried out in air at room temperature using a NanoWizardIII atomic force microscope (JPK Instruments), while the data were analyzed using SurfaceXplorer and JPKSPM Data Processing software. The AFM images were collected using a V-shaped silicon cantilever (spring constant of 3 N/m, tip curvature radius of 10.0 nm and the cone angle of 20°) operating in a contact mode.

The X-ray diffraction measurements at grazing incidence (XRDGI) were performed using a D8 Discover diffractometer (Bruker) with Cu K ($\lambda = 1.54 \text{ \AA}$) X-ray source. Parallel beam geometry with 60 mm Göbel mirror (X-ray mirror on a high precision parabolic surface) was used. This configuration enables transforming the divergent incident X-ray beam from a line focus of the X-ray tube into a parallel beam that is free of K radiation. Primary side also had a Soller slit with an axial divergence of 2.5°. The secondary side had a LYNXEYE (1D mode) detector with an opening angle of 2.16° and slit opening of 6.0 mm. Sample stage was a Centric Eulerian cradle mounted to horizontal D8 Discover with a vacuum chuck (sample holder) fixed on the top of the stage. X-ray generator voltage and current was 40.0kV and 40mA, respectively. The XRDGI scans of emitting layers were performed in the range of 3-134.0° with a step size of 0.065°, time per step of 19.2 s and

auto-repeat function enabled. The XRDGI scans were performed at incidence angle of 1.0°. *Processing of the resultant diffractograms was performed with DIFFRAC.EVA software.*

Results and Discussion

Synthesis, thermal and photophysical properties

The routes of the synthesis of the derivatives of 2-phenylindole and carbazole are shown in Scheme 1. In the first step, the mixture of 2-phenylindole-3-carbaldehyde and 9*H*-carbazole was treated with HCl to obtain the intermediate compound **CPIC**. 2-Phenylindole-3-carbaldehyde was reduced to 3-hydroxymethyl-2-phenylindole (**HMPI**) which was then condensed with 2-phenylindole and 9-ethylcarbazole to obtain **BPIM** and **PIMC** respectively. The last step in the synthesis of the target compounds was the introduction of the reactive functional groups by the interaction of the intermediate products with the corresponding halides in the presence of potassium *tert*-butoxide. All the target compounds were purified by column chromatography and characterized by spectroscopic tools and elemental analysis. They were found to be soluble in common organic solvents.

<Insert Scheme 1.>

Thermal properties of the derivatives were investigated by thermogravimetric (TG) analysis and differential scanning calorimetry (DSC). The thermal characteristics of compounds **1–5** are collected in Table 1. TG curves and differential thermogravimetric (DTG) curves are presented in Fig.1a, b. The temperatures of the onsets of the thermal degradation of most of the compounds were found to be rather moderate. They were found in the interval from 228 to 284 °C, while that of compound **5** was considerably higher (404 °C).

<Insert Figure 1>

Compounds **2** and **4** were isolated as crystalline substances. Their melting points were found to be 110 °C and 120 °C, respectively. It was not possible to transform them to the glassy state by cooling from the melts. Compounds **1**, **3** and **5** were isolated as amorphous materials. The glass transition temperatures of compounds **3** and **5** were found to be 134 °C and 85 °C respectively. The higher glass transition temperature of compound **3** can be explained by its higher molecular weight which determines stronger intermolecular interaction in the solid state. We did not manage to detect glass transition temperature of compound **1**. In DSC heating scan it showed only sharp endothermic signal at 246 °C due to sublimation.

<Insert Table 1>

UV-vis spectra of the dilute solutions of compounds **1**, **4** and **5** representing two different families of the derivatives of 2-phenylindole and carbazole are shown in Fig. 2. The wavelengths of absorption maxima of the compounds (**1–5**) are summarized in Table 2.

<Insert Figure 2>

The derivatives absorb UV-vis radiation in the range from 200 to 375 nm. The absorption bands observed in the region of 250–270 nm can be ascribed to the localized aromatic π - π^* transitions of 2-phenylindole moiety while those appeared in the region of 275–330 nm can be assigned to a localized aromatic π - π^* transition of carbazole species. The wavelengths of absorption bands of the solutions of the compounds increase in the order **1** > **4** > **5**. The optical band gap values estimated from the absorption band edges of the solutions of compounds **1–5** are in the range from 3.29 to 3.46 eV. Compound **5** showed the lowest value of optical band gap (3.29 eV). These values are lower than the theoretically calculated optical band gap values that range from 4.35 eV to 4.92 eV.

<Insert Table 2>

Emission spectra recorded at room and at low (77 K) temperatures of the dilute solutions of compounds **1–5** are shown in Fig.3. The wavelengths of photoluminescence (PL) intensity maxima are summarized in Table 2.

<Insert Figure 3>

PL spectra are characterized by the single peak at *ca.* 359 nm for the solutions of compounds **1** and **3**, at 363 nm for the solutions of compounds **2** and **4**, and at 381 nm for the solution of compound **5**. Similarly, as in the case of absorption spectra, the wavelengths of fluorescence intensity maxima of the solutions increase in the order of **1** > **4** > **5**. The observed fluorescence can be attributed to the relaxation of the excited states in which the whole molecules are involved. The triplet energy levels established for the dilute solutions of the monomers from their phosphorescence spectra at 77 K reach 3.02–3.04 eV for 2-phenylindolylcarbazolylmethane derivatives **1–3** and 2.91 eV and 2.88 eV for compounds **4** and **5**. These values are much higher than those previously reported for other host materials such as indole-carbazole hybrids (2.62–2.99 eV) [17] and triindolylmethanes (2.97–2.99 eV) [9].

Electrochemical and electron photoemission properties

Electrochemical properties of the compounds were investigated by cyclic voltammetry (CV). The resulting data are summarized in Table 2. As an example, cyclic voltammograms of compound **1** are shown in Fig. 4.

<Insert Figure 4>

All the studied compounds showed irreversible oxidation suggesting electrochemical coupling. During the multiple scans new reversible oxidation peaks at around 0.65 V were observed for all the compounds. It was found that the onset oxidation potential was much lower for the 2-phenylindolylcarbazolylmethane derivative **5** than for 2-phenylindole twin compound **4** which may be due to the strong electron donating origin of the carbazole moiety. The solid-state ionization

potential (IP_{CV}) and electron affinity (EA_{CV}) values were estimated from the oxidation onset potentials ($E_{ox\ onset\ vs.Fc}$) and optical band gaps (E_g^{opt}). The ionization potential values of compounds **1-5** established by CV were found to be in the short range of 5.50–5.84. The electron affinity values ranged from 2.12 to 2.45 eV.

The ionization potentials of the solid samples of compounds **1-5** were estimated by the electron photoemission spectrometry in air. Electron photoemission spectra are shown in Fig. 5 and the results are summarized in Table 2.

<Insert Figure 5>

The values of ionization potentials recorded by electron photoemission spectrometry were found to be close to those estimated by CV and ranged from 5.74 eV to 5.88 eV. Monomer **5** showed the lowest ionization potential (5.45 eV). This result correlates with UV spectrometry data which showed the lowest value of E_g^{opt} for compound **5**.

Results of computational study

Quantum chemical calculations were performed for compounds **1-5** using DFT/B3LYP/ 6-31 (d, p) method. The optimized structures revealed that the carbazole and 2-phenylindole moieties in all the compounds are set in the different planes. Fig. 6 shows the molecular orbital plots of the optimized structures of **1-5**. π -Electrons in the HOMO orbitals of the 2-phenylindolylylcarbazolylmethane derivatives **1-3** and **5** are delocalized over all carbazole-indole backbone, except phenyl- moiety, whereas the HOMO orbital of the indole twin derivative **4** is delocalized over both indole moieties with the same exception of the phenyl group. The LUMO orbitals of **1, 4** and **5** are delocalized over vinylbenzyl fragment, while those of compounds **2** and **3** are delocalized on carbazole moieties (Fig. 6). The smallest energy gap, which was experimentally observed for compound **5**, indicates the most extensive π -electron delocalization among the series. Although DFT calculations show that delocalization of HOMO orbitals of the compound **5** are

similar to that of compound **1**, the absence of the additional carbazole moiety in **5** has impact on its photophysical and photoelectrical properties.

<Insert Figure 6>

Polymerization

Photocross-linking of monomers **1** and **4** was studied by ATR-FTIR spectrometry. For the measurements the solution of a monomer (0.5M) containing 3 mol % of photoinitiator cyclopentadienyl(fluorene)iron(II)hexafluorophosphate was drop-casted on the surface of ATR-FTIR analysis crystal, the solvent was vaporized by heating at 40 °C for 15 min and then the monitoring of the decrease of the intensity of the absorption band of vinyl group under exposure of UV radiation source was performed.

<Inset Figure 7>

Fig. 7 shows the fragments of FTIR spectra of the films of compounds **1**(a) and **4** (b) at the different stages of photocuring. They illustrate the decrease of the intensity of absorption bands of vinyl groups at 997 cm^{-1} with the increase of the time of photocuring (photocured for 15 min). The values of the insoluble fractions of the obtained materials were found to be 76 % and 56 %, respectively (estimated after the extraction of the samples with chloroform for 24h).

Polymerization of monomer **5** was performed in solution, and the product was characterized by gel chromatography. The weight average relative molecular weight was determined to be 1870 and number average molecular weight was of 1110. The thermal degradation temperature (474 °C) of the product was determined by TG (see Fig. S3) and it was 70 °C degrees higher than the monomer **5** onset degradation temperature (404 °C). The glass transition temperature (120 °C) obtained from the DSC curves is 62 °C degrees higher than the monomer glass transition temperature (58 °C).

Charge-transporting and device properties

Charge-transporting properties of the solid layers of **2** and **5** were studied by the method of space-charge-limited current (SCLC) [18]. The hole-only devices with the following architectures were fabricated: ITO/m-MTDATA(20 nm)/ **2** or **5** (80 nm)/m-MTDATA(20 nm)/Al(60 nm). The layer of m-MTDATA (4,4',4''-tris[3-methylphenyl(phenyl)amino]triphenylamine) was used as the hole-injecting and electron-blocking layer. The current density vs. voltage characteristics of the hole-only devices are plotted in Fig. 1. The values of hole mobility were estimated using the Mott-Gurney law [18]:

$$J_{SCLC} = \mu_{SCLC} \frac{9}{8} \epsilon \epsilon_0 \frac{V^2}{d^3}, \quad (1)$$

where J_{SCLC} is the steady-state current density (SCLC), μ_{SCLC} is the SCLC mobility; V is applied voltage; d is the film thickness, ϵ is the permittivity of the film (~ 3); ϵ_0 is the absolute permittivity of the free space.

<Insert Figure 8>

The similar current density vs. voltage dependencies were observed for compounds **2** and **5** (Fig.8). Values of the zero-field hole mobility of $1.97 \times 10^{-5} \text{ cm}^2 \text{V}^{-1} \text{s}^{-1}$ and $1.78 \times 10^{-5} \text{ cm}^2 \text{V}^{-1} \text{s}^{-1}$ for **2** and **5**, respectively, were obtained by fitting the region (III), in which the SCLC occurred, of the experimental current density vs. voltage curve with Eq. 1 (Fig. 8). The disagreement between the experimental and fit curves can be explained by taking in account the existence of hole traps in **2** and **5** which can occur due to volume or morphology effects in solid state layers [19]. Additional explanation of that can be the absent Ohmic contact, which is required for SCLC method, in the hole-only and electron-only devices [18]. The region I is the Ohmic region while the region II can be caused by injection-limited behavior, trap filling, or built-in voltage [18].

To study the performance of **2** and **5** as hosts, the simple PhOLEDs were fabricated. In the devices with the structures ITO/m-MTDATA (25 nm)/**2** or **5**:Ir(ppy)₃(15 nm)/Bphen (30 nm)/Ca:Al (devices A and B, respectively), 4,4',4''-tris[phenyl(m-tolyl)amino]triphenylamine (m-MTDATA) was used as the hole-transporting material and 4,7-diphenyl-1,10-phenanthroline (Bphen) was

utilized as the electron-transporting material. To prepare the emitting layers **2**:Ir(ppy)₃ and **5**:Ir(ppy)₃ for the devices A and B, the hosts **2** and **5** were doped with tris[2-phenylpyridinato-C2,N]iridium(III) (Ir(ppy)₃) as a green phosphorescent emitter. Efficient exciton confinement on the dopant Ir(ppy)₃ was expected due to relatively high triplet levels of 3.02 eV and 2.88 for **2** and **5** (Table 2) [20].

The electroluminescence (EL) spectra of the devices A and B are shown in Figure 8. The fabricated PhOLEDs were characterized by green emissions with the intensity maxima at ca. 510 nm, confirming the radiative recombination of excitons on Ir(ppy)₃. However, low intensity blue emissions with the intensity maxima at ca. 430 nm were observed in EL spectra of both PhOLEDs. The wavelengths of these emissions were close to that of photoluminescence of m-MTDATA showing that the recombination of excitons occurred not only in the emitting layers but also in the hole-transporting layer of devices A and B. To avoid the recombination of excitons in the hole-transporting layer, either additional electron-blocking layer or exciton-blocking layer are required [21]. The similar shapes of EL spectra at the different applied voltages for both the devices were observed. However, intensity of the blue emissions increased in the EL spectra of the PhOLEDs with the increase of the applied voltage. The CIE coordinates were (0.29; 0.59) and (0.35; 0.64) which were calculated for the EL at 8 V of the devices A and B, respectively. The better colour purity was observed for device A.

<Insert Figure 9>

The luminance and efficiency characteristics of the devices A and B are plotted in Figure 10. Both the devices were characterized by the relatively low values of the turn-on voltage ($V_{on}=3.7$ for device A and $V_{on}=3.1$ V for device B), confirming the very efficient injection from the electrodes and transport of holes and electrons to the emission layers (Figure 11). The driving voltage of 4.9 V at 1000 cd/m² was observed for device B and it was by 1 V lower than that observed for device A (Figure 10 a). This observation indicates the better charge balance in device B than in device A,

owing the better charge injection due to the more appropriate HOMO and LUMO levels (Figure 11). The higher maximum brightness of ca. 11900 cd/m² was recorded for device B than that observed for device A (5700 cd/m²) (Figure 10). The higher brightness and lower driving voltages observed for the device B compared to those recorded for the device A shows more effective exciton recombination and radiative transition in the emitting layer with the host **5**. [22]

<Insert Figure 10>

The efficiency curves of the PhOLEDs are shown in Figure 10 b-d. The devices A and B based on hosts **2** and **5** exhibited the maximum current efficiency, power efficiency, and external quantum efficiency of 4.2 and 10.3 cd/A, 2.5 and 7.2 lm/W, 1.2 and 2.9 % respectively in the absence of light out-coupling enhancement. The external quantum efficiencies of 1.05 and 2.24 % at 1000 cd/m² were recorded (Figure 10 b-d) showing the efficiency roll-offs of 12.5 and 22.7 % for the devices A and B respectively. The external quantum efficiencies of PhOLEDs decreased at high current density and high exciton concentration apparently due to the unbalanced charges and quenching effects. [22] We noted that the simple and unoptimized PhOLEDs based on hosts **2** and **5** were fabricated, therefore, the maximum efficiencies of devices A and B were lower compared to those reported for PhOLEDs containing Ir(ppy)₃ [23,21,24]. The better performance of the devices based on the hosts **2** and **5** can apparently be reached either after introduction of the additional layers, after the additional optimization of the concentration of dopant Ir(ppy)₃ in hosts **2** and **5**, or after the additional optimization of the thicknesses of the layers of the devices.

<Insert Figure 11>

Since the triplet energy levels of **2** and **5** were found to be high, they were tested as the host materials for the blue phosphorescent emitter bis[2-(4,6- difluorophenyl) pyridinato -C2,N] (picolinato)iridium(III) (FIrpic). We fabricated blue PhOLEDs with structures ITO/m-MTDATA (25 nm)/**2** (5nm)/**2** or **5**:FIrpic (15 nm)/DPEPO(5 nm)/Bphen (30 nm)/Ca:Al (devices C and D, respectively). DPEPO is an abbreviation of Bis[2-(diphenylphosphino)phenyl] ether oxide which

was used from a site of electron injection as the exciton-blocking material with a high triplet level (3.3 eV). An additional layer **2** was also used as the exciton-blocking layer from the other site of the emitting layer. Such multilayer structure did not allow to obtain effective blue PhOLEDs since the additional emission band was observed in the low energy region of the EL spectra (Figure 12). The emission with the maxima at 470 and 503 nm is related to pure Irpic emission while the low energy maximum apparently results from intermolecular system (an exciplex or an electroplex) formed in the emitting layer. Taking into account this observation for the blue PhOLED, the shoulders in the EL spectra of the green PhOLEDs can be identified only after the careful analysis. Those shoulders can also be assigned to exciplex or electroplex emission. Recently the phosphorescence exciplex between tri(9-hexylcarbazol-3-yl)amine and Irpic was reported [25].

<Insert Figure 12>

Morphology of the layers

AFM measurements were performed for vacuum deposited light-emitting layers **2**:Ir(ppy)₃ and **5**:Ir(ppy)₃ on glass substrates. The AFM topographical images are shown in Fig. 13. The topography of **2**:Ir(ppy)₃ shows relatively homogeneous surface with morphological features having a mean height of 1.18 nm and the root mean square roughness (R_q) of 0.36 nm. The surface of **2**:Ir(ppy)₃ is dominated by the peaks with skewness (R_{sk}) value of 0.79 and has a leptokurtic distribution of the morphological features with kurtosis (R_{ku}) value of 4.67 indicating relatively many high peaks and low valleys. In contrast to **2**:Ir(ppy)₃, the **5**:Ir(ppy)₃ surface was found to be more rough with randomly oriented surface mounds having a mean height of 3.60 and R_q value of 1.24 nm. The surface of **5**:Ir(ppy)₃ exhibited relatively similar symmetry and leptokurtic distribution of the morphological features with R_{sk} and R_{ku} values of 0.58 and 4.42, respectively. Both, light-emitting layers **2**:Ir(ppy)₃ and **5**:Ir(ppy)₃ exhibited quite low roughness values which are acceptable for structuring OLEDs as the low roughness values of host:guest emission layers contribute to the higher brightness and efficiency of PhOLEDs [26].

<Insert Figure 13>

The X-ray diffraction patterns at grazing incidence angle of 1.0° of **2**:Ir(ppy)₃ and **5**:Ir(ppy)₃ thin films are shown in Fig. S2. The broad reflex at about $2\theta = 23.6^\circ$ in both diffractograms indicates amorphous character of thin films. Since crystallization and aggregation significantly affect the device stability and lifetime, amorphous layers as those of **2**:Ir(ppy)₃ and **5**:Ir(ppy)₃ are favourable for OLEDs [27]. In addition, the amorphous materials exhibit the excellent processability, homogeneity and isotropic properties, which are also required for the highly efficient OLEDs [28].

Conclusions

2-Phenylindole and carbazole derivatives were synthesized and studied as highly-efficient hosts for phosphorescent OLEDs. Photopolymerization of the compounds having vinylbenzyl reactive functional groups was demonstrated in the solid films and in solutions. The compounds with high triplet energies of 3.02 and 2.88 eV as well as with favourable for charge injection HOMO/LUMO values were tested as the hosts in blue and green phosphorescent OLEDs. The green devices demonstrated practically pure emission of the used dopant, the relatively low values of the turn-on voltages of 3.7 and 3.1 V as well as the efficiency roll-offs of 12.5 and 22.7 %. Light-emitting layers of green PhOLEDs based on the synthesized hosts exhibited low roughness values and amorphous character. The best green device exhibited the maximum current, power, and external quantum efficiencies of 10.3 cd/A, 7.2 lm/W, 2.9 %, respectively, in the absence of light outcoupling enhancement. Electroluminescence of the blue device was related not only to pure emission of the dopant but also to exciplex and/or electroplex emission formed between host and guest.

Acknowledgments

Financial support from the Research Council of Lithuania (project No. TAP LB-03/2015) is gratefully acknowledged.

References

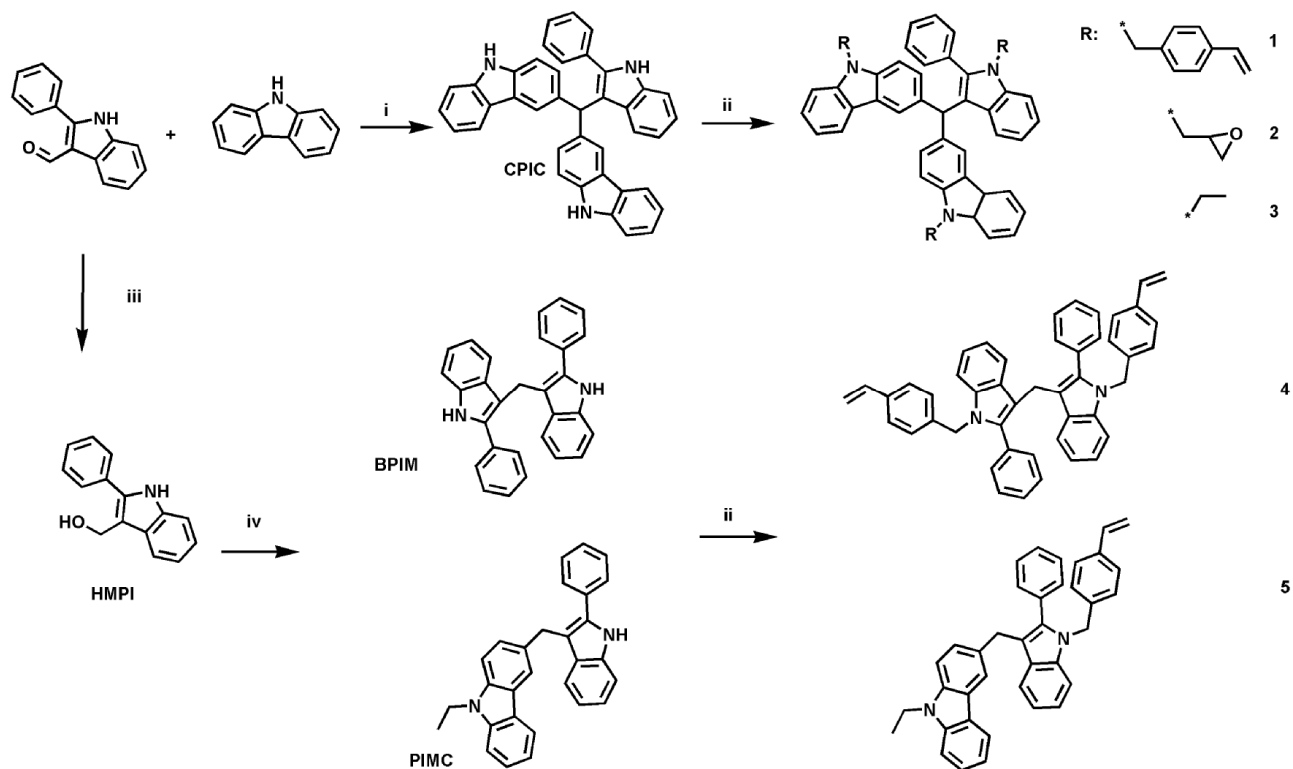
-
- [1] Minaev B., Baryshnikov G., Agren H. Principles of phosphorescent organic light emitting devices. *Phys. Chem. Chem. Phys.* 2014;16:1719–58. Doi: 10.1039/c3cp53806k
- [2] Adachi C., Baldo M., Thompson M.E., Forrest S.R.J. Nearly 100% internal phosphorescence efficiency in an organic light-emitting device. *Appl. Phys.* 2001;90:5048–51. Doi: dx.doi.org/10.1063/1.1409582
- [3] Huang J.H., Su J. H., Tian H. The development of anthracene derivatives for organic light-emitting diodes, *J. Mater. Chem.*, 2012;22: 10977-10989. Doi: 10.1039/c2jm16855c
- [4] Lia J., Grimsdale A. C. Carbazole-based polymers for organic photovoltaic devices. *Chem. Soc. Rev.* 2010;39:2399–10. Doi:10.1039/B915995A
- [5] Huang J. H. Su J.H., Li X., Lam M. K., Fung K.M., Fan H.H., Cheah K.W., Chen C.H., Tian H. Bipolar anthracene derivatives containing hole- and electron-transporting moieties for highly efficient blue electroluminescence devices, *J. Mater. Chem.* 2011;21: 2957-2964
- [6] Dumur F. Carbazole-based polymers as hosts for solution-processed organic light emitting diodes: simplicity, efficacy. *Org. Electron.* 2015;25:345–61. Doi:0.1016/j.orgel.2015.07.007
- [7] Stanislovaityte E., Simokaitiene J., Raisys S., Al-Attar H., Grazulevicius J. V., Monkman A. P., Jankus V. Carbazole based polymers as hosts for blue iridium emitters: synthesis, photophysics and high efficiency PLEDs. *J. Mater. Chem. C.* 2013;1:8209-21. Doi:10.1039/C3TC31441C
- [8] Dumur F., Beouch L., Peralta S., Wantz G., Goubard F., Gigmes D. Solution-processed blue phosphorescent OLEDs with carbazole-based polymeric host materials. *Org. Electron.* 2015;25:21–30. Doi: 10.1016/j.orgel.2015.06.013
- [9] Kirkus M., Lygaitis R., Tsai M.H., Grazulevicius J.V., Wu C.C. Triindolylmethane-based high triplet energy glass-forming electroactive molecular materials. *Synthetic Met.* 2008;158:226–32. Doi:10.1016/j.synthmet.2008.01.006

- [10] Leete E. 3-Hydroxymethylindoles. *J. Am. Chem. Soc.* 1959;81:6023–26.
Doi:10.1021/ja01531a042
- [11] Kruzinauskiene A., Matoliukstyte A., Michaleviciute A., Grazulevicius J.V., Musnickas J., Gaidelis V., Jankauskas V. Carbazolyl- and diphenylamino substituted fluorenes as hole transport materials. *Synthetic Met.* 2007;157:401–06.
Doi:dx.doi.org/10.1016/j.synthmet.2007.04.007
- [12] Miyamoto E., Yamaguchi Y., Yokoyama M. Ionization potential of organic pigment film by atmospheric photoelectron emission analysis. *Denshishashin Gakkai-shi (Electrophotography)* 1989;28:364–70. Doi: 10.11370/isjepj.28.364
- [13] Kukhta N.A., Volyniuk D., Peciulyte L., Ostrauskaite J., Juska G., Grazulevicius J.V.. Structure property relationships of star-shaped blue-emitting charge-transporting 1,3,5-triphenylbenzene derivatives. *Dyes Pigm.* 2015;117:122–32. Doi:10.1016/j.dyepig.2015.02.013
- [14] Gritzner G., Kuta J. Recommendations on reporting electrode potentials in nonaqueous solvents. *Pure Appl. Chem.* 1984;56:461–66. Doi:dx.doi.org/10.1351/pac19845604046
- [15] SPARTAN'14 for Windows Version 1.1.2. 1840 Von Karman Avenue, Suite 370, Irvine, CA 92612: Wavefunction, Inc.; 2013.
- [16] Okamoto, S.; Tanaka, K.; Izumi, Y.; Adachi, H.; Yamaji, T.; Suzuki, T. Simple Measurement of Quantum Efficiency in Organic Electroluminescent Devices. *JPN J A P 2* 2001;40:L783–84.
Doi:10.1143/JJAP.40.L783
- [17] Kirkus M., Tsai M.H., Grazulevicius J.V., Wu C.C., Chi L.C., Wong K.T. New indole-carbazole hybrids as glass-forming high-triplet-energy materials. *Synthetic Met.* 2009;159:729–34. Doi:10.1016/j.synthmet.2008.12.027
- [18] Blakesley J.C., Castro F.A., Kylberg W., Dibb G.F., Arantes C., Valaski R., Cremona M., Kim J.S., Kim J.-S. Towards reliable charge-mobility benchmark measurements for organic semiconductors. *Org Electron* 2014;15:1263–72. Doi: 10.1016/j.orgel.2014.02.008

- [19] Angioni E., Chapran M., Ivaniuk K., Kostiv N., Cherpak V., Stakhira P., Lazauskas A., Tamulevicius S., Volyniuk D., Findlay N.J., Tuttle T., Grazulevicius J.V., Skabara P.J. A single emitting layer white OLED based on exciplex interface emission. *J. Mater. Chem. C* 2016;4:3851–56. Doi: 10.1039/C6TC00750C
- [20] Tomkute-Luksiene D., Keruckas J., Malinauskas T., Simokaitiene J., Getautis V., Grazulevicius J.V., Volyniuk D., Cherpak V., Stakhira P., Yashchuk V., Kosach V., Luka G., Sidaravicius J.. 2-Phenyl-1,2,3-benzotriazole Ir(III) complexes with additional donor fragment for single-layer PhOLED devices. *Dyes Pigm.* 2013;96:278–86. Doi: 10.1016/j.dyepig.2012.08.012
- [21] He G., Pfeiffer M., Leo K., Hofmann M., Birnstock J., Pudzich R., Salbeck J. High-efficiency and low-voltage p-i-n electrophosphorescent organic light-emitting diodes with double-emission layers. *Appl. Phys. Lett.* 2004;85:3911–13. Doi: 10.1063/1.1812378
- [22] Zhang Z., Zhang Z., Ding D., Wei Y., Xu H, Jia J., Zhao Y., Pan K., Huang W. Selectively Investigating Molecular Configuration Effect on Blue Electrophosphorescent Host Performance through a Series of Hydrocarbon Oligomers. *J. Phys. Chem. C* 2014;118:20559–70. Doi: 10.1021/jp506513x
- [23] Baldo M. A., Thompson M. E., Forrest S. R. High-efficiency fluorescent organic light-emitting devices using a phosphorescent sensitizer. *Nat.* 2000;403:750–53. Doi:10.1038/35001541
- [24] Keruckas J., Grazulevicius J.V., Volyniuk D., Cherpak V., Stakhira P.. 3,6-Bis(indol-1-yl)-9-phenylcarbazoles as electroactive materials for electrophosphorescent diodes. *Dyes Pigm* 2014;100:66-72. Doi.org/10.1016/j.dyepig.2013.07.020
- [25] Cherpak V., Stakhira P., Minaev B., Baryshnikov G., Stromylo E., Helzhynskyy I., Chapran M., Volyniuk D., Hotra Z., Dabulienė A., Tomkeviciene A., Voznyak L., Grazulevicius J.V. Mixing of Phosphorescent and Exciplex Emission in Efficient Organic Electroluminescent Devices. *ACS Appl. Mater. Interfaces* 2015;7:1219–1225. Doi: 10.3116/16091833/16/2/95/2015

- [26] Bagdziunas G., Grybauskaite G., Kostiv N., Ivaniuk K., Volyniuk D., Lazauskas A. Green and red phosphorescent organic lightemitting diodes with ambipolar hosts based on phenothiazine and carbazole moieties: photoelectrical properties, morphology and efficiency. *RSC Adv.*, 2016, 6, 61544–61554. Doi: 10.1039/c6ra12692h
- [27] Sun Y.-H., Zhu X.-H., Chen Z., Zhang Y., Cao, Y. Potential Solution Processible Phosphorescent Iridium Complexes toward Applications in Doped Light-Emitting Diodes: Rapid Syntheses and Optical and Morphological Characterizations. *J. Org. Chem.*, 2006;71:6281–6284. Doi: 10.1021/jo060840h.
- [28] Shirota Y., Kageyama H. Charge Carrier Transporting Molecular Materials and Their Applications in Devices. *Chem. Rev.*, 2007;107:953–1010. Doi: 10.1021/cr050143+.

SCHEMES



Scheme 1.

FIGURES

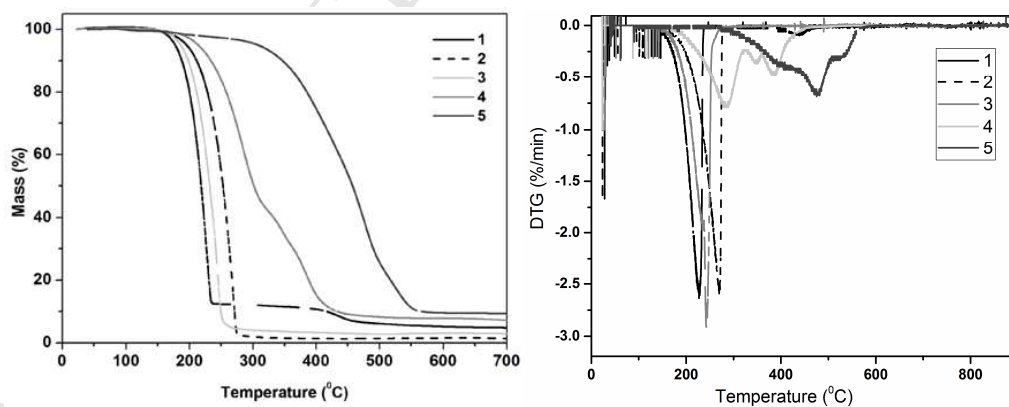


Figure Error! Main Document Only..

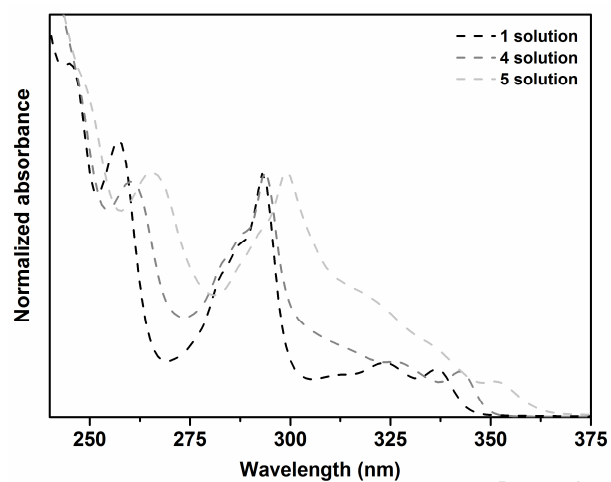
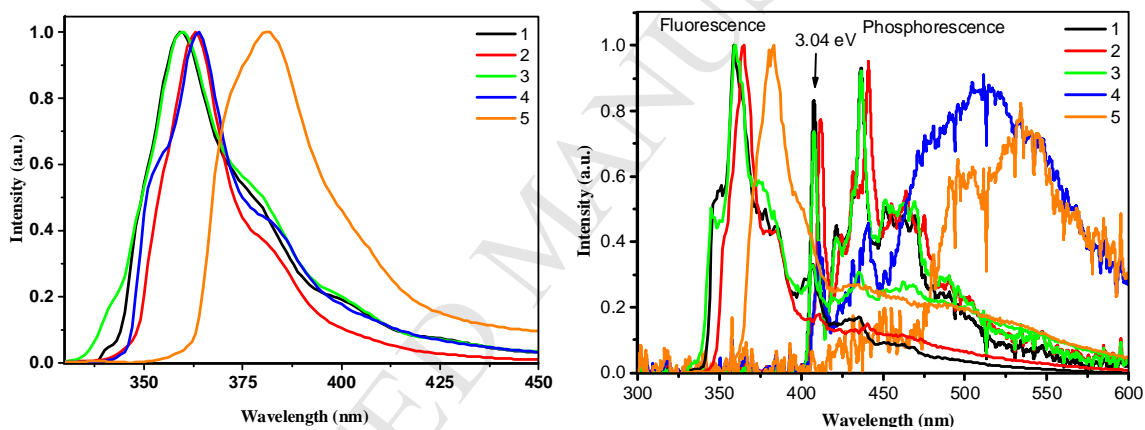


Figure Error! Main Document Only..



a)

b)

Figure Error! Main Document Only..

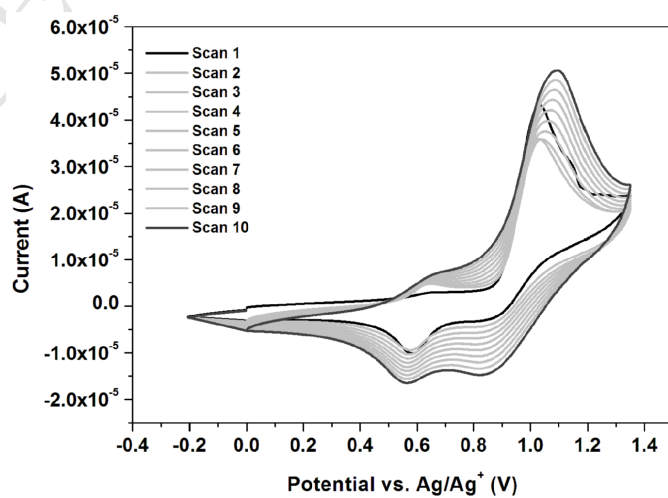


Figure Error! Main Document Only..

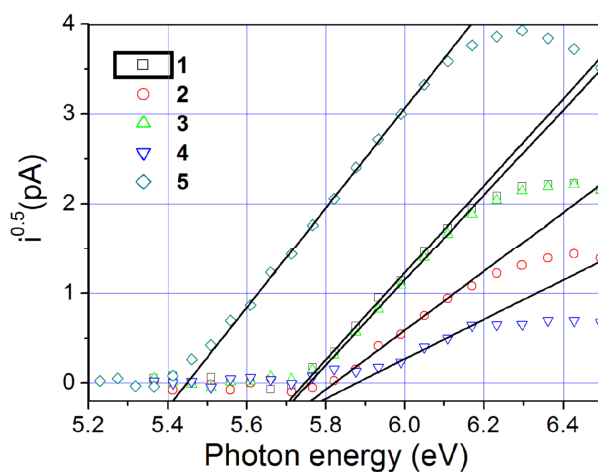


Figure Error! Main Document Only..

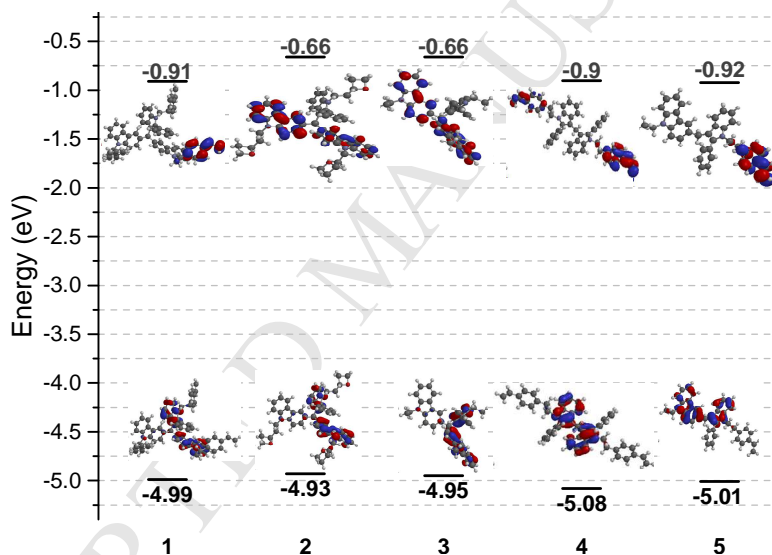


Figure Error! Main Document Only..

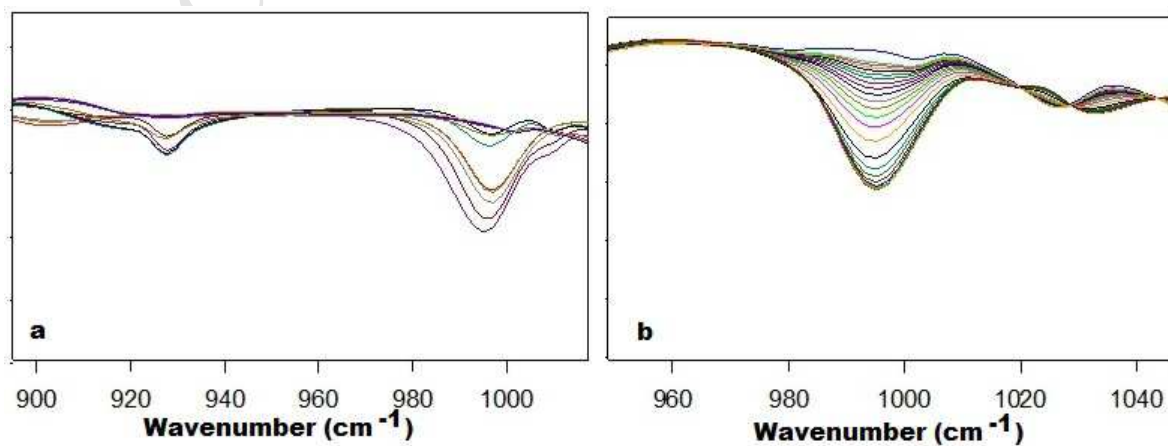


Figure Error! Main Document Only..

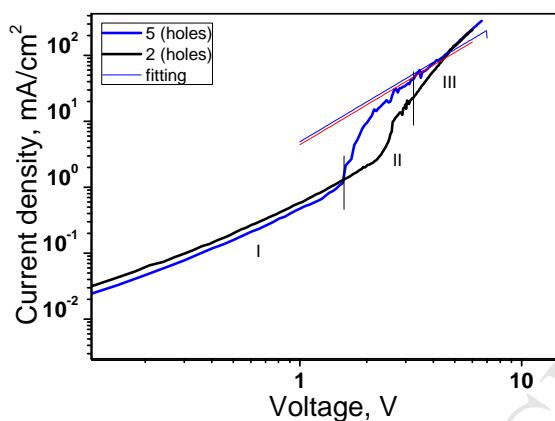


Figure Error! Main Document Only..

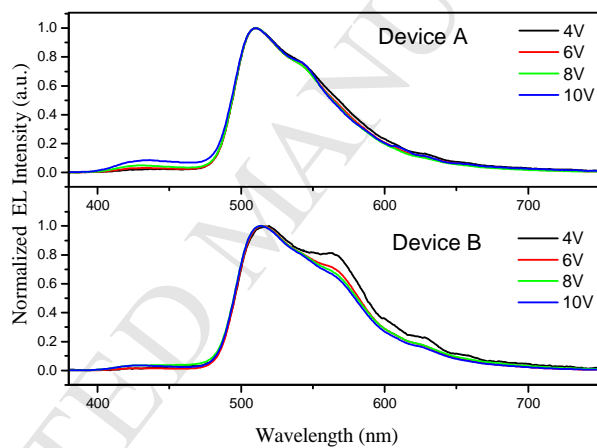
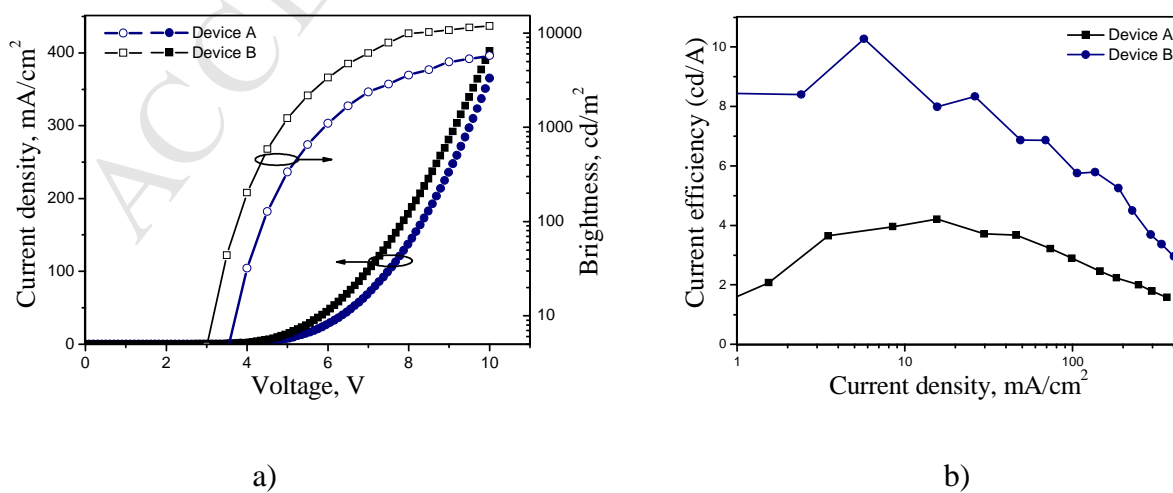


Figure 9.



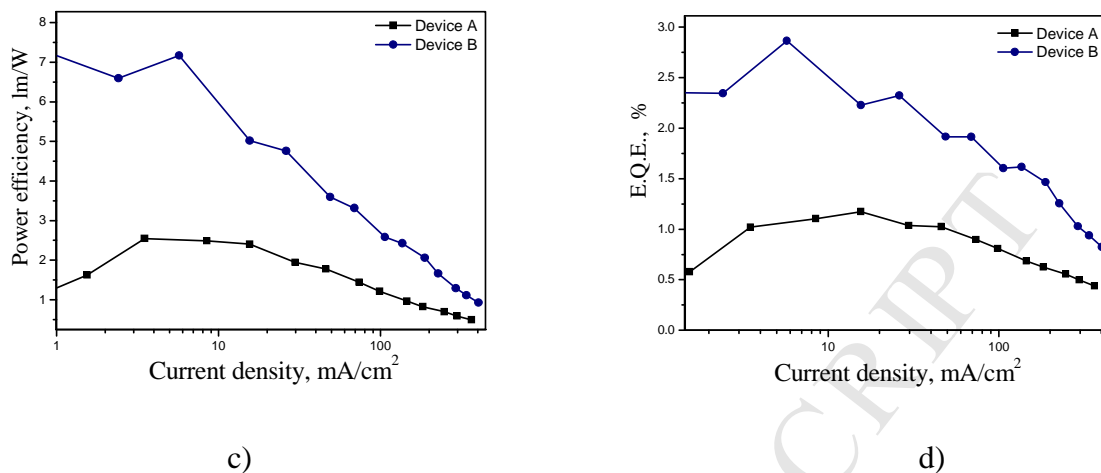


Figure 10.

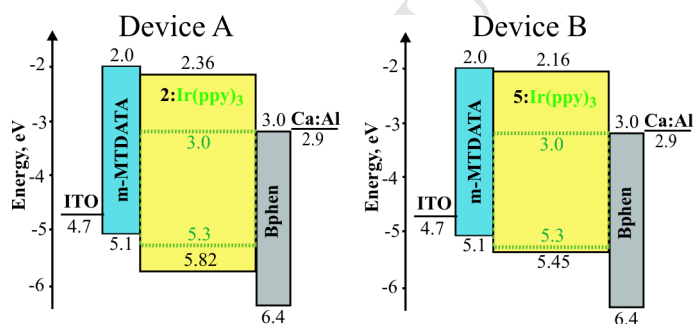


Figure 11.

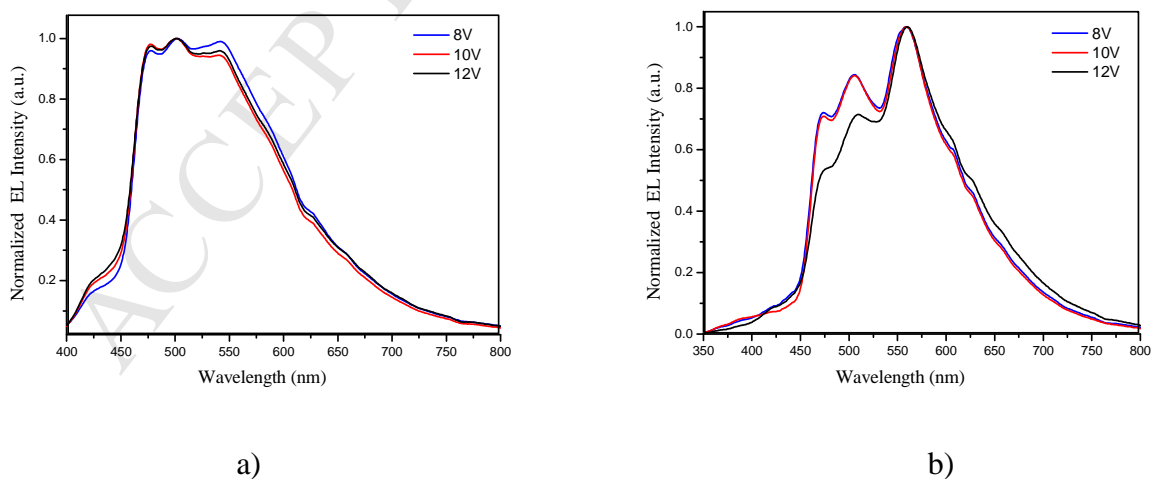


Figure 12.

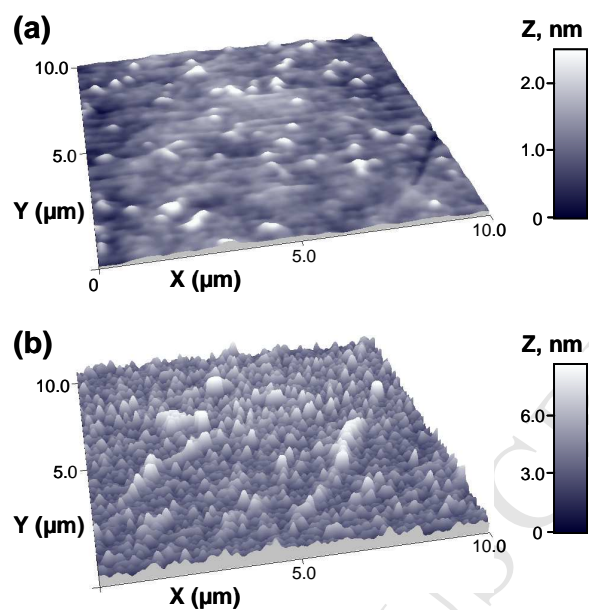


Figure 13.

TABLES

Table 1. Thermal properties of compounds 1–5.

Compound	T_m^a , °C	T_g^b , °C	T_{cr}^c , °C	T_{ID}^d , °C
1	-	- ^e	-	228
2	110	-	54	242
3	-	134	-	268
4	120	-	-	284
5	-	85	-	404

^a - melting point observed at the first heating scan of the DSC measurement;

^b - glass transition temperature recorded by DSC;

^c - crystallization observed during DSC cooling scan;

^d - initial weight loss temperature obtained from TG curves;

^e - not detected.

Table 2. Photophysical and electrochemical characteristics of compounds 1–5.

	Compound	1	2	3	4	5
Solution	$\lambda_{\text{Abs}}^{\text{a}}$, nm	259, 298, 325,337	259,298, 325,341	259,298, 325,336	360, 298, 327,342	262, 301, 352
	$\lambda_{\text{PL}}^{\text{b}}$, nm	359	363	359	363	381
	E_{S1}^{c} , eV	3.45	3.42	3.45	3.42	3.25
	Stokes shift ^d , nm	40	22	25	22	81
	$\lambda_{\text{PH}}^{\text{e}}$, nm	407	410	407	425	430
	E_{T1}^{f} , eV	3.04	3.02	3.04	2.91	2.88
	$\Delta E_{\text{ST}}^{\text{g}}$, eV	0.41	0.40	0.41	0.51	0.37
	$E_{\text{ox onset vs.Fc}}^{\text{h}}$, V	0.73	0.52	0.42	0.71	0.40
	IP^{i} , eV	5.74	5.82	5.74	5.88	5.45
	$\text{IP}_{\text{CV}}^{\text{j}}$, eV	5.83	5.62	5.52	5.81	5.50
	$E_{\text{g}}^{\text{opt k}}$, eV	3.42	3.46	3.40	3.36	3.29
	$\text{EA}_{\text{CV}}^{\text{l}}$, eV	2.41	2.16	2.12	2.45	2.21
	HOMO ^m , eV	-4.99	-4.93	-4.95	-5.08	-5.01
	LUMO ⁿ , eV	-0.91	-0.66	-0.66	-0.90	-0.92
	E_{g}^{o} , eV	4.08	4.27	4.29	4.63	4.35

^a - absorption maxima;

^b - emission maxima;

^c - singlet energy calculated from $1240/\lambda_{\text{PL}}$;

^d - $\lambda_{\text{PL}} - \lambda_{\text{Abs}}$;

^e - phosphorescence maxima;

^f - triplet energy calculated from $1240/\lambda_{\text{PH}}$;

^g - energy gap between E_{S1} and E_{T1} ;

^h - onset oxidation potential of the sample vs. onset oxidation potential of ferrocene;

ⁱ - ionization potential estimated by electron photoemission spectrometry;

^j - ionization potential, $\text{IP}_{\text{CV}} = E_{\text{onset ox vs.Fc}} + 5.1$ eV [28, 28];

^k - optical band gap calculated from $1240/\lambda_{\text{Abs onset}}$ (onset absorption);

^l - electron affinity, $\text{EA}_{\text{CV}} = \text{IP}_{\text{CV}} - E_{\text{g}}^{\text{opt}}$;

^m - theoretically calculated HOMO energy;

ⁿ - theoretically calculated LUMO energy;

^o - HOMO-LUMO.

FIGURE CAPTIONS

Scheme 1. Synthesis of 2-phenylindolylcarbazole derivatives. (i) HCl (conc.), tetrahydrofuran/methanol, r.t., 5h; (ii) alkylhalide, K-*t*BuO, BTMAC, DMSO, r. t., 48h; (iii) NaBH₄, methanol, 0-5 °C, 2 h; (iv) 9-ethylcarbazole or 2-phenylindole, BF₃ • Et₂O, dichloromethane, 3 h.

Figure 1. TG (a) and DTG (b) curves of 2-phenylindolo-carbazole derivatives 1–5. (Heating rate 10 °C/min, N₂ atm).

Figure 2. The absorption spectra of the dilute THF solutions of compounds 1, 4 and 5.

Figure 3. Photoluminescence spectra recorded at room temperature (a); the photoluminescence (thick curves) and phosphorescence (thin curves) spectra recorded at 77 K (b) of the dilute THF solutions of compounds 1–5. $\lambda_{\text{ex}} = 320$ nm.

Figure 4. Cyclic voltammograms of compound 1.

Figure 5. Electron photoemission spectra of compounds 1–5.

Figure 6. Molecular orbital plots (B3LYP/ 6-31G**) of compounds 1–5.

Figure 7. The fragments of FTIR spectra recorded during photocuring of the films of compounds 1(a) and 4 (b) containing 3 mol % of cyclopentadienyl(fluorene)iron(II)hexafluorophosphate.

Figure 8. Current density vs voltage characteristics of the hole-only devices based on the 2 and 5 layer.

Figure 9. EL spectra of PhOLEDs recorded at the different applied voltages.

Figure 10. EL characteristics of devices A and B: current density and luminance versus voltage (a), current efficiency versus current density (b), power efficiency versus current density (c), external quantum efficiency versus current density (d).

Figure 11. Energy-band diagrams of devices A and B.

Figure 12. EL spectra of the devices C (a) and D (b) recorded at the different applied voltages.

Figure 13. AFM topographical images with normalized Z axis in nm of light-emitting layers of 2:Ir(ppy)₃ (a) and 5:Ir(ppy)₃ (b). The images were acquired in air using contact mode.

- New derivatives of carbazole and 2-phenylindole.
- Photopolymerization was demonstrated by ATR-FTIR.
- The triplet energy levels were found to be in the range of 2.88-3.04 eV.
- The hole mobility values exceed $1.78 \times 10^{-5} \text{ cm}^2 \text{V}^{-1} \text{s}^{-1}$.
- The materials were used as hosts in green OLEDs.

ACCEPTED MANUSCRIPT